Response to Reviewer 1

(comments in red, responses in black)

Dear Reviewer,

We thank the Reviewer for the careful evaluation and constructive comments. In response, we returned to the underlying experimental records, re-examined the disputed quantitative analyses, corrected several data-processing and interpretation issues, and revised the manuscript accordingly. Where the archived measurements allowed, we re-derived the relevant quantitative results and added additional consistency checks; where the available measurements did not support the original causal interpretation, we revised the interpretation to reflect the evidence actually available.

The manuscript has also been retitled “Design and Characterization of a Cloud Chamber for Warm- and Cold-Cloud Microphysical Studies.” The revised study focuses on chamber design and characterization, thermodynamic response during depressurization, integrated aerosol and cloud-droplet measurements, and repeated warm- and cold-cloud formation experiments.

Major Comment 1

Reproducibility and the term "quantitative" (carried over from access review, point 1 - not addressed)

Required: either (a) provide replicate paired experiments with run-to-run spread for at least the two demonstration cases, or (b) remove "Quantitative" from the title, remove "reproducible framework" from the conclusions, and attach uncertainty estimates (instrument + repeatability) to every quoted number. As written, the central claim of the paper is unsupported by its evidence base.

Response

The original single background–seeded pairs did not provide run-to-run variability sufficient for quantitative seeding-effect claims. Each seeding condition in the original manuscript was represented by only a single background–seeded pair, so the manuscript did not provide the replication or run-to-run variability required for such claims.

In response to the Reviewer’s Required revision, we have followed option (b). “Quantitative” has been removed from the title, and the former statement describing the system as a “reproducible framework for quantitative seeding experiments” has been removed from the Conclusions. Accordingly, the former single-run seeding-effect quantities are no longer used to support quantitative causal conclusions in the revised manuscript.

The revised Results instead present four warm-cloud and two cold-cloud experiments conducted without deliberate seeding or standard-aerosol addition. These experiments are used

only to characterize chamber-operation consistency under the tested conditions and are not interpreted as evidence of seeding-effect reproducibility. For repeated quantitative chamber-characterization results that remain in the revised manuscript, run-to-run variability is reported where appropriate, for example as mean ± SD for the four repeated warm-cloud thermodynamic responses. To implement option (b), repeated chamber-characterization results are reported as mean ± SD with the number of runs stated, whereas single-test values are identified as characterization measurements and accompanied by manufacturer specifications where available. Repeatability cannot be estimated for unreplicated tests; these values are not presented as reproducible performance metrics or seeding effects.

Major Comment 2

The seeding signal is confounded by the delivery method - no blank-injection control (new)

Required: (a) report injection duration, injected volume, carrier-gas dew point, and temperature for both experiments; (b) perform and present blank-injection controls (carrier air only; and for the cold case, a burnt blank without AgI, or at minimum carrier-air-only) - this is the obvious and necessary control for the paired design; (c) discuss the mismatch in cooling rates and its consequences; (d) reconcile the opposite-sign RH-decline logic between Sects. 3 and 4.

Response

The original experiments did not separate material effects from delivery-induced thermodynamic perturbations. We agree that the original paired experiments did not fully separate the effect of the seeding material from the perturbation introduced by the delivery process.

(a) Injection parameters. In the original experiments, the exact injection duration, total injected gas volume, carrier-gas dew point, and delivery temperature were not recorded with sufficient completeness for a quantitative thermodynamic correction. These quantities therefore cannot be reconstructed reliably from the archived records.

(b) Blank-injection controls. Carrier-gas-only and combustion-blank controls were not included in the original paired experiments. We agree that such controls are necessary to distinguish a delivery-induced perturbation from the effect of the introduced material.

(c) Cooling-rate mismatch. Re-examination of the original records confirmed that the background and seeded cases followed different cooling histories. Because droplet activation and cloud evolution depend directly on the thermodynamic trajectory, this mismatch represents an additional confounding factor and prevents the cooling-rate difference from being attributed uniquely to the seeding material.

(d) RH interpretation. We therefore no longer interpret either a faster or a slower RH decline as

evidence of a seeding response. Once the delivery perturbation and different thermodynamic histories are considered together, the sign of the RH-slope difference is not physically diagnostic of a material effect.

The original paired experiments therefore do not provide an identifiable quantitative estimate of the material effect because the delivery perturbation and thermodynamic evolution were not independently controlled. Future controlled seeding experiments will record delivery duration, carrier-gas volume, temperature and dew point, and will include carrier-only and, for AgI, combustion-blank controls under matched thermodynamic trajectories.

Major Comment 3

The reported saturation ratios are physically impossible and internally contradictory (new; arises from the response to access-review point 4)

Required: remove or completely rework the saturation-ratio analysis. Characterize the LI-COR's in-cloud response (or restrict it to cloud-free periods), state which temperature record enters the calculation, propagate uncertainties, and reconcile the result with the co-plotted RH sensor. As it stands, this addition undermines rather than supports the paper's credibility - and the access-review request for a discussion of the supersaturation limitation remains effectively unmet.

Response

The large discrepancy between the LI-COR-derived saturation ratio and the simultaneous chamber RH record prompted us to re-examine both the calculation and the measurement configuration. We agree that the former $S = 1.222$ value should not have been interpreted quantitatively without validating the water-vapour and temperature measurements under cloudy, near-saturated conditions.

Previous cloud-chamber studies show that saturation ratio is fundamentally a coupled water-vapour–temperature measurement problem. Anderson et al. (2021), for example, determined saturation ratio in the Π Chamber using simultaneous water-vapour and temperature measurements selected to represent comparable spatial and temporal scales. Moteki and Kondo (2013) developed a thermodynamic method for estimating temperature and saturation ratio in expansion chambers from measurable thermodynamic variables. In the present chamber, the revised thermodynamic analysis shows substantial non-adiabatic heat exchange during depressurization, so direct application of an adiabatic expansion formulation is not sufficient to determine the actual in-cloud saturation state. Together, these studies show that saturation ratio depends on spatially compatible water-vapour and temperature measurements. Because no temperature sensor was collocated with the LI-COR sampling volume and the LI-COR and KYWS-SX were not cross-calibrated under cloud-containing conditions, the spatial-

representativeness and in-cloud response terms cannot be estimated from the archived data. Propagating nominal sensor specifications alone would therefore give a misleading uncertainty for S. We removed $S = 1.222$ and do not report a replacement in-cloud saturation ratio.

(a) Saturation-ratio calculation. Re-examination of the original analysis showed that the saturation ratio was calculated from the LI-COR water-vapour measurement together with the mean air temperature from the three chamber temperature levels. This introduces a representativeness problem because the LI-COR provides a local water-vapour measurement, whereas the three-level mean temperature represents a spatially averaged chamber temperature. The revised chamber analysis further shows mean inter-level temperature ranges of approximately 0.87–1.01 °C during the warm-cloud runs and 1.15–1.27 °C during the cold-cloud runs. Because saturation vapour pressure is highly temperature sensitive, this temperature inhomogeneity is sufficient to produce several percentage points of local RH variation near saturation. We therefore regard the former$S = 1.222$ value as quantitatively invalid for the measurement configuration used, rather than simply as a value with large uncertainty.

(b) LI-COR response under cloudy conditions. The LI-COR water-vapour measurement had not been independently characterized for quantitative use under cloud-containing, near-saturated conditions. This distinction is important because established chamber measurements distinguish between local/interstitial water vapour and total-water measurements in the presence of condensed particles. AIDA hygrometer intercomparisons provide an example of dedicated water-vapour characterization under high-humidity conditions (Brunamonti et al., 2025). We therefore do not use the present LI-COR record to derive a quantitative in-cloud supersaturation.

(c) A numerical reconciliation is not attempted because the LI-COR and KYWS-SX were not cross-calibrated under cloud-containing conditions and did not represent the same measurement volume. Their disagreement therefore indicates that the archived records cannot support a quantitative in-cloud saturation ratio. The KYWS-SX is retained for local operational RH monitoring, while neither sensor is used to infer quantitative in-cloud supersaturation.

We therefore removed the former saturation-ratio calculation and its associated supersaturation interpretation. For future saturation-ratio measurements, we will intercompare the LI-COR 7500DS and KYWS-SX with a chilled-mirror dew-point hygrometer under cloud-free, near-saturated, and cloud-containing conditions, and future saturation-ratio calculations will use water-vapour and air-temperature measurements that are spatially and temporally collocated as closely as practicable. Uncertainty propagation will then include contributions from both water-vapour pressure and temperature.

Major Comment 4

The 1357 cm^-3 (droplets >= 12 um) value fails a basic water budget (carried over from access

review, point 7 - not addressed, now sharpened)

Required: state the instrument, time window, and size bins behind 1357 and 478 cm^-3; provide the corresponding time series and total concentrations; provide an LWC closure estimate; and correct or withdraw the value. Since 1357 -> 478 is the abstract's headline warm-cloud result, this must be resolved with raw data, not adjusted wording.

Response

Re-examination of the FM-120 export identified a bin-count/concentration error in the former ≥12 µm calculation. In response, we returned to the original FM-120 export files and re-examined the calculation from the raw 1 s records. This re-analysis identified the source of the inconsistency in the original calculation. The FM-120 raw export reports the total particle number concentration ("Number Conc (#/cm³)") separately from the 30 Fog Monitor Bin variables, together with LWC and MVD.

In the original analysis, the summed values of the 30 bin variables were inadvertently treated as bin-resolved number concentrations. Re-examination of the raw files showed that these variables are the particle-count histogram for each 1 s record rather than concentrations in cm^{-3}. Consequently, the previously reported values of 1357 and 478 cm^{-3} were not valid number concentrations and are corrected here.

The original analysis intervals were recovered by matching the archived bin-resolved records to the FM-120 raw files. The background interval contained 421 consecutive 1 s records from 14:17:59.98 to 14:24:59.98, and the seeded interval contained 441 consecutive 1 s records from 14:49:54.89 to 14:57:14.84. For each record, the bin-resolved number concentration was recalculated from the instrument-reported total number concentration and the fractional particle count in each bin,

$$N_i = N_{\mathrm{tot}} \frac{C_i}{\sum_j C_j}$$

where C_i is the FM-120 count in size bin i. The ≥12 µm concentration was calculated from the nominal diameter bins 12, 13, 14, 16, 18, 20, 22, 24, 26, 28, 30, 32, 34, 36, 38, 40, 42, 44, 46, 48, and 50 µm.

Using this corrected calculation, the mean total droplet concentrations over the analysed intervals were 2906 cm^{-3} for the background experiment and 1534 cm^{-3} for the seeded experiment. The corresponding mean concentrations for droplets ≥12 µm were 413 and 146 cm^{-3}, respectively. Thus, the former values of 1357 and 478 cm^{-3} are withdrawn and replaced by the concentrations obtained directly from the original FM-120 concentration output and size-bin count distributions.

We also performed the water-budget check requested by the Reviewer. Over the same analysis

intervals, the FM-120 reported mean LWCs of 1.354 g m^{-3} for the background experiment and 0.589 g m^{-3} for the seeded experiment, with corresponding mean MVDs of 11.92 and 12.03 μm. As an internal consistency check, LWC was separately reconstructed from the corrected bin-resolved number concentrations assuming spherical water droplets and using the nominal channel diameters:

$$\mathrm{LWC_{PSD}} = \frac{\pi}{6}\rho_w \sum_i N_i D_i^3$$

The reconstructed mean LWCs were 1.589 and 0.690 g m^{-3}, respectively, approximately 17% higher than the corresponding FM-120-reported values in both experiments. Given that this reconstruction uses nominal channel diameters rather than the instrument's internal size representation, we regard the agreement in magnitude and the nearly identical relative difference between the two experiments as an internal water-budget consistency check, rather than as an independent LWC validation.

Figure R4. Re-analysis of the original FM-120 measurements for the background and seeded warm-cloud experiments. (a) Total droplet number concentration, (b) number concentration of droplets with nominal diameters ≥12 μm, and (c) FM-120-reported liquid water content (LWC).

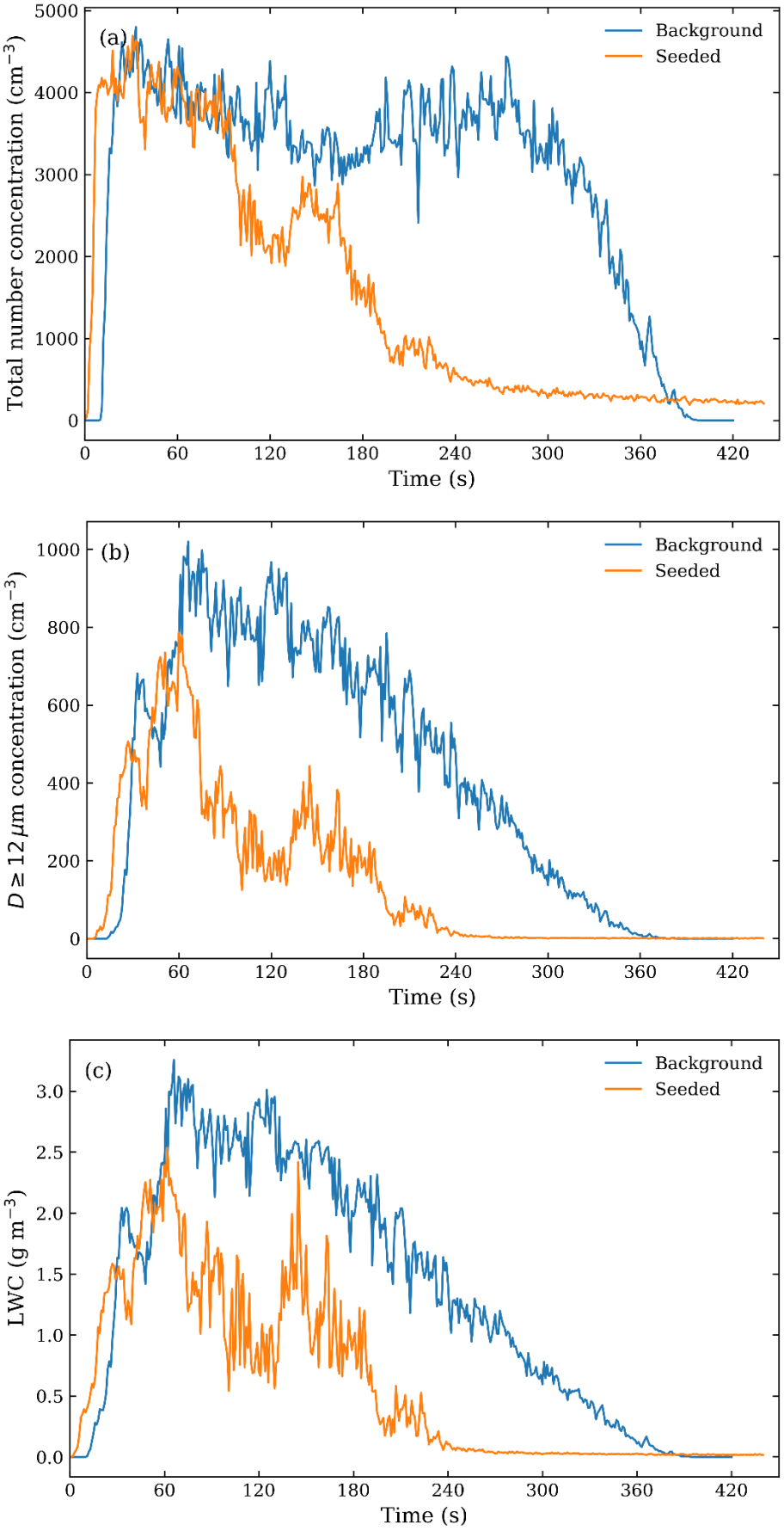
(a)
Background
Seeded
Total number concentration (cm^{-3})
5000
4000
3000
2000
1000
0
0
60
120
180
240
300
360
420
Time (s)
(b)
Background
Seeded
$D \geq 12\,\mu$m concentration (cm^{-3})
1000
800
600
400
200
0
0
60
120
180
240
300
360
420
Time (s)
(c)
Background
Seeded
LWC (g m^{-3})
3.0
2.5
2.0
1.5
1.0
0.5
0.0
0
60
120
180
240
300
360
420
Time (s)

The corresponding 1 s time series of total number concentration, ≥12 μm number concentration, and LWC are provided in Fig. R4. These results resolve the original water-budget inconsistency by identifying and correcting the bin-count/concentration error from the raw FM-120 records. Because the original comparison was based on a single background–seeded pair, however, the corrected concentrations are reported here to resolve the Reviewer's quantitative concern and are not used in the revised manuscript to infer a causal seeding effect.

Major Comment 5

Ice-phase identification remains qualitative, and the shown data are internally inconsistent (carried over from access review, point 2 - not addressed, now stronger)

Required: reconstructed hologram images with a stated focus/shape classification criterion; the number of holograms and particles analysed, with a false-positive assessment; an ice number concentration time series; CUIT-CIP images/concentrations; a consistency check of HCDS-derived concentrations against the droplet probes; and a serious treatment of the liquid-only alternative. Without quantitative ice detection, the cold-cloud section demonstrates aerosol injection followed by cloud decay - not glaciogenic seeding.

Response

We agree that the two representative holographic images shown in the original manuscript were insufficient, by themselves, to establish particle phase. We therefore returned to the retained HCDS outputs and re-examined both the phase-identification procedure and the quantitative results available from the original experiment.

The HCDS used in this experiment was the same digital-holographic instrument used by Yang et al. (2024). The measurements were processed using the established automated analysis software developed at Xi'an University of Technology. The published workflow includes numerical hologram reconstruction, focus determination, particle extraction, and morphology-based phase classification, including a roundness criterion for distinguishing ice-crystal and liquid-droplet images. Yang et al. (2024) reported recognition exceeding 93% under the specified roundness-based classification criterion. We cite this result as method-level validation of the established HCDS procedure, rather than as an experiment-specific false-positive rate for the present chamber measurements.

We then re-examined the retained processed HCDS outputs from the approximately 1 min cloud-formation interval analysed in the original AgI experiment. The dataset contains 59 consecutive 1 s processed records, with separate outputs for particles classified as ice crystals and liquid droplets, including number concentration, MVD, and 30-bin size distributions. During this interval, the ice-classified population had a mean number concentration of 12.8 ± 3.3 cm^{-3}, compared with 45.4 ± 8.1 cm^{-3} for the liquid-droplet population. The corresponding

mean MVD values were 36.7 and 21.5 μm, respectively. The summed 30-bin concentrations also reproduce the reported total number concentration for each 1 s record. The corresponding concentration and MVD time series are shown in Fig. R5.

Figure R5. HCDS phase-classified particle measurements during the approximately 1 min cloud-formation interval analysed in the original AgI experiment. (a) Number concentrations of particles classified as ice crystals and liquid droplets and (b) corresponding median volume diameters (MVDs).

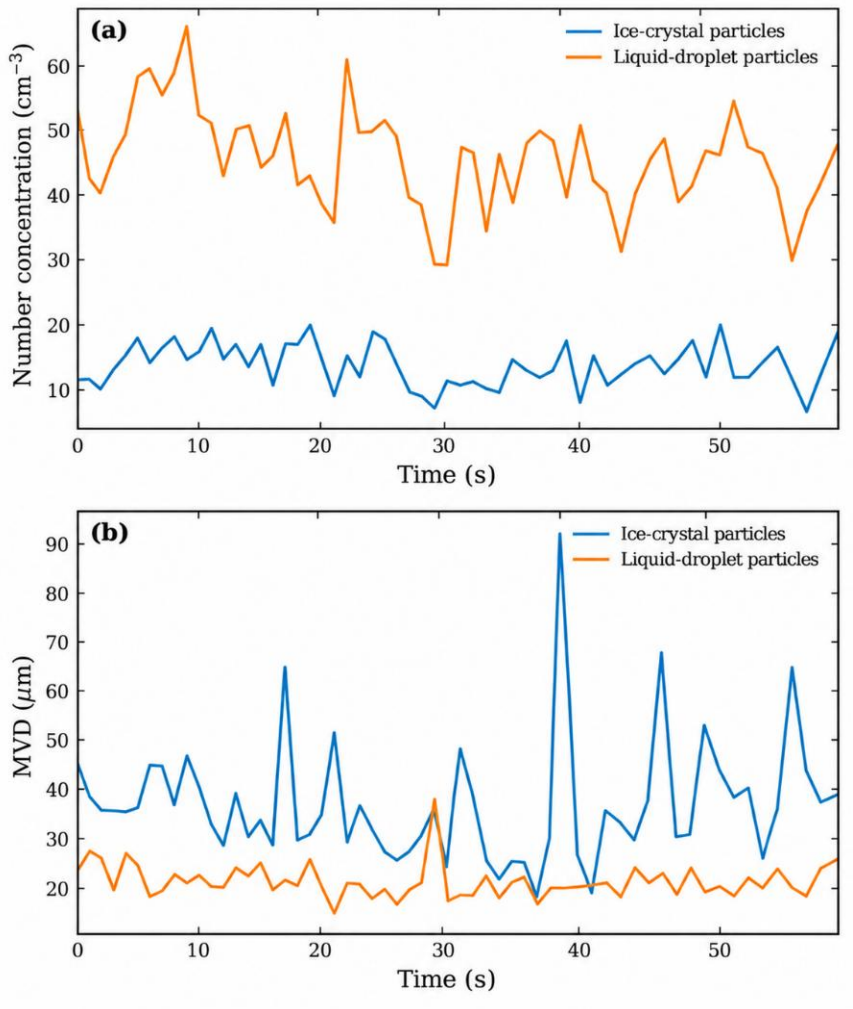

The 59 values represent processed 1 s outputs, not 59 individual holograms. Because the archived working dataset does not retain the complete acquisition-level record needed to reconstruct the total number of individual holograms and particles contributing to these 1 s products, we do not infer those numbers retrospectively. Likewise, an experiment-specific false-positive assessment was not independently performed for this interval.

We also examined the additional cross-instrument validation requested by the Reviewer. A synchronized quantitative CUIT-CIP phase comparison was not available, and a one-to-one concentration closure between the HCDS and the droplet probes could not be established

because the retained measurements do not share a matched observation volume and synchronized sampling basis. Consequently, these measurements do not provide an independent experiment-specific verification of every HCDS phase label, and the liquid-only alternative is not treated as excluded solely by the present chamber dataset.

Nevertheless, the retained HCDS dataset provides a quantitative phase-resolved time series of distinct software-classified ice and liquid particle populations, rather than only the two qualitative images shown in the original manuscript. We therefore retain the HCDS time series as supporting evidence for particle-phase differentiation during the analysed cloud-formation interval, while not using it to calculate a quantitative AgI glaciation efficiency or an experiment-specific ice-activation fraction.

Major Comment 6

AgI activity at the achieved temperatures, and the injection timeline (carried over from access review, point 3 - not addressed)

Required: a full timeline (t_injection vs t_expansion vs t_cloud) for all four runs; the minimum in-cloud temperature; a comparison with DeMott (1995); the AgI dosage definition and stick composition.

Response

We re-examined the original 1 s thermodynamic records and experimental logs to reconstruct the timing of seeding-material introduction and cloud-forming depressurization in all four original experiments. The reconstructed sequence is summarized in Table R6.

(1) Injection–expansion timeline. Here, $t_{\mathrm{injection}}$ denotes the onset of seeding-material introduction, whereas $t_{\mathrm{expansion}}$ denotes the onset of the sustained depressurization used to generate the cloud. For the two background experiments, $t_{\mathrm{injection}}$ is not applicable because no seeding material was introduced.

In the warm-cloud background experiment, cloud-forming depressurization began at approximately 14:18. In the warm-cloud seeded experiment, depressurization began at approximately 14:49:55, and the hygroscopic seeding material was introduced approximately 10 s later, at about 14:50.

In the cold-cloud background experiment, the cloud-forming depressurization began at approximately 16:07. In the cold-cloud AgI experiment, the sequence was different. The first pressure-decrease/recovery cycle, beginning at approximately 16:28, was used to introduce the combustion-generated aerosol. Chamber pressure decreased from approximately 943 to 921 hPa and subsequently recovered to approximately 946 hPa. The subsequent sustained cloud-forming depressurization began at approximately 16:42 and reduced the chamber pressure to

approximately 710 hPa by about 16:47.

A unique t_{cloud} was not assigned retrospectively because visual cloud onset was not independently time-stamped and no specific cloud-onset criterion had been defined in the original experimental protocol. The FM-120 was operated in situ in the designated lower observation region and provides time-resolved measurements of cloud-particle evolution, but its first detected droplet signal was not predefined as the chamber cloud-onset time. We therefore report the directly reconstructable $t_{\mathrm{injection}}$ and $t_{\mathrm{expansion}}$ rather than introducing a new retrospective definition of t_{cloud}.

Table R6. Reconstructed timing of seeding-material injection and cloud-forming depressurization in the four original experiments.

Experiment	$t_{\mathrm{injection}}$	$t_{\mathrm{expansion}}$	t_{cloud}
Warm-cloud background	N/A	~14:18	Not independently defined
Warm-cloud seeded	~14:50	~14:49:55	Not independently defined
Cold-cloud background	N/A	~16:07	Not independently defined
Cold-cloud AgI	~16:28	~16:42	Not independently defined

The detailed injection–expansion sequences of the two seeded experiments are additionally shown in Fig. R6.

Figure R6. Particle-size distributions and pressure and air-temperature evolution during the cold-cloud AgI (a, c) and warm-cloud hygroscopic-seeding (b, d) experiments.

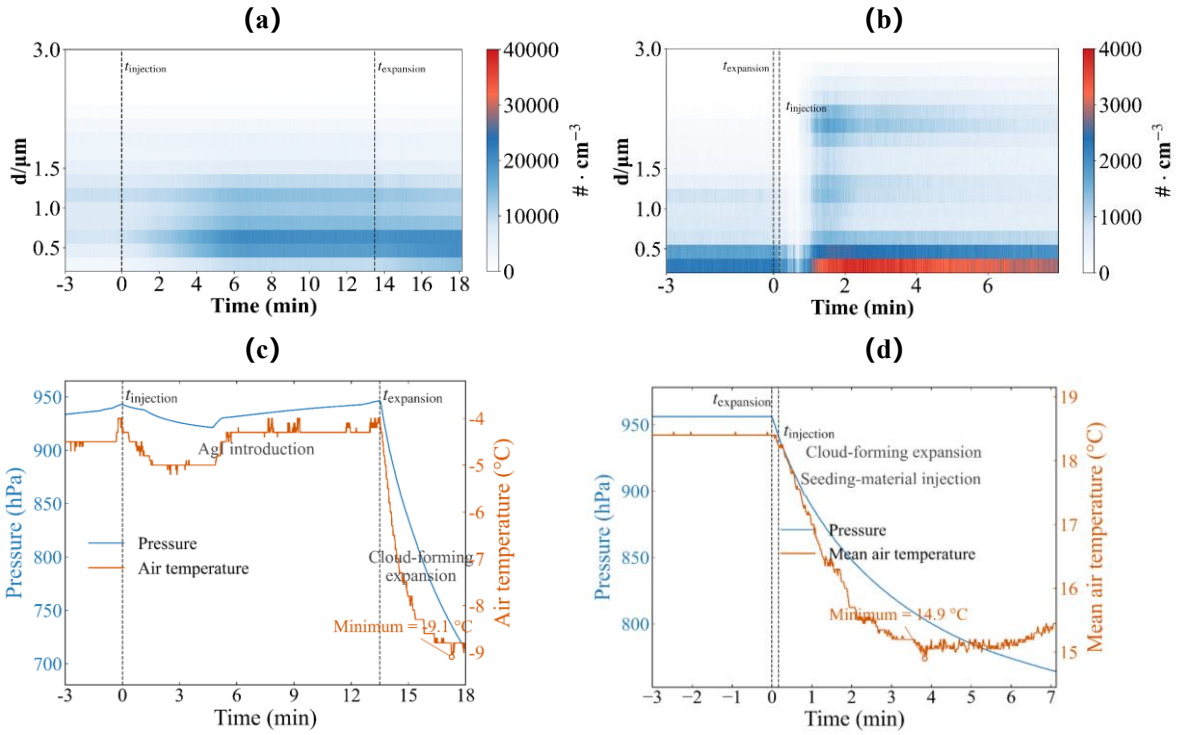

(2) Minimum temperature. During the AgI-associated cloud-forming depressurization, the recorded chamber air temperature decreased from approximately −4 °C at the onset of depressurization to a minimum recorded value of −9.1 °C. The corresponding unseeded cold-cloud background experiment reached a similar minimum temperature of approximately −8.6 °C.

(3) Comparison with DeMott (1995). We agree that the ice-nucleating activity of AgI-type aerosols is strongly temperature dependent. The original AgI experiment reached a minimum recorded temperature of approximately −9 °C. However, DeMott (1995) also shows that AgI activity depends on aerosol properties and cannot be inferred from temperature alone. Because the number concentration, size distribution, and active fraction of the combustion-generated AgI-containing aerosol were not independently measured, a quantitative AgI activation efficiency cannot be derived from the present experiment.

(4) AgI dosage and flare composition. The experiment used a commercially manufactured YF-4 aircraft flare produced by Shaanxi Zhongtian Rocket Technology Co., Ltd. The reported 0.5 g refers to the actual mass of combustion material consumed during the experiment, rather than the mass of pure AgI. Because a batch-specific AgI mass fraction and the particle-number/size distribution of the combustion-generated aerosol were not independently determined, this 0.5 g combustion-material dose cannot be converted reliably into a net AgI mass dose or particle-number dose.

Major Comment 7

Humidity sensing near saturation (carried over from access review, point 4 - not addressed)

Response

We appreciate the Reviewer's concern regarding humidity measurements under cloudy and near-saturated conditions. We agree that the KYWS-SX measurement should be interpreted as a local RH measurement rather than as an exact chamber-volume-mean humidity state.

The KYWS-SX sensor is installed approximately 1.5 m above the bottom of chamber B. The measured chamber-temperature structure also provides a quantitative indication of the spatial representativeness of the RH measurement. During cloud-forming depressurization, the mean inter-level temperature ranges were approximately 0.87–1.01 °C for the four warm-cloud runs and 1.15–1.27 °C for the two cold-cloud runs. Near saturation, a local temperature deviation of approximately ±0.5–1 °C corresponds to roughly ∓3–7 percentage points in equilibrium RH at fixed water-vapour pressure. Thus, spatial thermal inhomogeneity alone can produce several percentage points of local RH variation within the chamber.

We therefore use the KYWS-SX measurements for local operational monitoring and chamber environmental characterization, rather than to infer an exact chamber-volume-mean supersaturation or small seeding-related RH differences.

Future tests will collocate temperature and water-vapour measurements and intercompare the KYWS-SX, LI-COR 7500DS, and DewStar under cloud-free and cloud-containing conditions.

Major Comment 8

"Adiabatic" framing vs strongly diabatic reality; consequences for the cloud-lifetime claims (new)

Response

We agree that the original description of the chamber depressurization as approximately adiabatic was not supported by the measured temperature response. We have therefore revised the thermodynamic interpretation and now compare the measured three-level mean air temperature with a dry-adiabatic reference calculated from the measured chamber pressure using the Poisson relation for dry air. The dry-adiabatic calculation is used only as a theoretical reference for evaluating the chamber response and is not interpreted as a description of the actual depressurization process.

For the six cloud-formation experiments retained in the revised manuscript, the measured cooling was substantially smaller than the dry-adiabatic reference. In the four warm-cloud runs, the measured temperature decreases were 2.1–2.3 °C, compared with 17.6–17.9 °C for the dry-adiabatic reference, corresponding to cooling ratios of 11.9–12.9 % (12.46 ± 0.48 %, mean ± SD, n = 4). In the two cold-cloud runs, the measured decreases were 2.1–2.2 °C, compared with

21.3–21.4 °C for the dry-adiabatic reference, giving cooling ratios of 10.0–10.4 %. Thus, the observed cooling amounted to only approximately 10–13 % of the corresponding dry-adiabatic reference. The revised quantitative comparison is reproduced below for clarity.

Revised Table 3. Comparison of measured and dry-adiabatic thermal responses during the repeated warm- and cold-cloud experiments.

Experiment	P_0 (hPa)	P_f(hPa)	ΔT_{obs} (°C)	ΔT_{da} (°C)	R_{cool}(%)	q''_{app}(W m^{-2})
Warm-cloud run 1	978.2	780.2	2.3	17.9	12.9	24.6
Warm-cloud run 2	975.4	779.8	2.2	17.8	12.2	24.7
Warm-cloud run 3	974.5	781.0	2.1	17.6	11.9	24.8
Warm-cloud run 4	973.5	778.1	2.3	17.9	12.9	24.6
Warm-cloud mean ± SD	975.4 ± 2.0	779.8 ± 1.2	2.22 ± 0.10	17.79 ± 0.13	12.46 ± 0.48	24.65 ± 0.10
Cold-cloud run 1	945.9	707.8	2.1	21.3	10.0	27.2
Cold-cloud run 2	942.7	704.8	2.2	21.4	10.4	26.7

To further characterize the chamber thermal response, we introduced a transient bulk control-volume energy analysis based on the measured $P(t)$ and three-level mean $T_g(t)$. Chamber B was treated as a rigid, lumped dry-air ideal-gas control volume with outflow only, with kinetic- and potential-energy terms neglected. Taking heat input to the chamber gas as positive and approximating the outflow enthalpy as $h_{\mathrm{out}} = c_p T_g$, the apparent heating rate was obtained from the transient control-volume energy equation combined with the ideal-gas relation. Pressure was evaluated in Pa and temperature in K. Equation (4) was evaluated from the 1 Hz measurements using finite differences between consecutive samples and then averaged over the analysed depressurization interval, excluding the subsequent ambient-air refill.

For area normalization, an estimated geometric internal surface area of chamber B was derived from the available manufacturer drawing. Using the manufacturer-specified internal diameter

of 1.8 m, an approximately 2.8 m cylindrical section, and the two ellipsoidal end sections shown in the drawing, the estimated area was approximately 22.6 m². The resulting area-normalized apparent diabatic heating was 24.6–24.8 W m^{-2} for the four warm-cloud runs and 26.7–27.2 W m^{-2} for the two cold-cloud runs. We emphasize that $\dot{Q}_{\mathrm{app}}$ represents the residual of a simplified dry-air bulk control-volume budget. This residual may include effects of wall and internal-component heat exchange, phase-change processes not explicitly represented in the dry-air formulation, and unresolved spatial transport. Accordingly, $\dot{Q}_{\mathrm{app}}$ and the corresponding area-normalized q''_{app} are interpreted as bulk diagnostic quantities rather than as direct measurements of wall heat flux.

The wall-temperature measurements provide independent evidence consistent with heat transfer from the relatively warm chamber boundaries to the cooling air. All ten wall-temperature sensors were used in the warm-cloud experiments; during the cold-cloud experiments, the lowest wall-temperature sensor was unavailable because of sensor malfunction, and the mean wall temperature was therefore calculated from the remaining nine valid sensors. In the four warm-cloud runs, the mean wall temperature exceeded the three-level mean air temperature during approximately 84.5–89.9 % of the analysed samples, with mean wall–air temperature differences of 0.55–0.84 °C; the corresponding mean differences in the two cold-cloud runs were 0.70 and 0.47 °C. The circulation fan was switched off during depressurization, and the measured inter-level temperature differences further indicated finite vertical thermal inhomogeneity. The mean inter-level temperature ranges were 0.87–1.01 °C in the four warm-cloud runs and 1.15–1.27 °C in the two cold-cloud runs. Accordingly, the former "adiabatic" or "nearly adiabatic" wording has been removed and the process is now described as depressurization cooling with substantial non-adiabatic thermal effects. Seeding-related interpretations based on differences in cloud persistence or dissipation have also been removed because these differences cannot be uniquely separated from the chamber thermodynamic response. The corresponding measured air-temperature, dry-adiabatic reference, and wall-temperature evolutions are shown in the revised Fig. 9 reproduced below.

Revised Figure 9. Comparison of measured mean air temperature T_g, dry-adiabatic reference temperature T_{da}, and mean wall temperature $\overline{T}_w$ during depressurization in chamber B. (a–d) Warm-cloud runs 1–4; (e–f) cold-cloud runs 1–2.

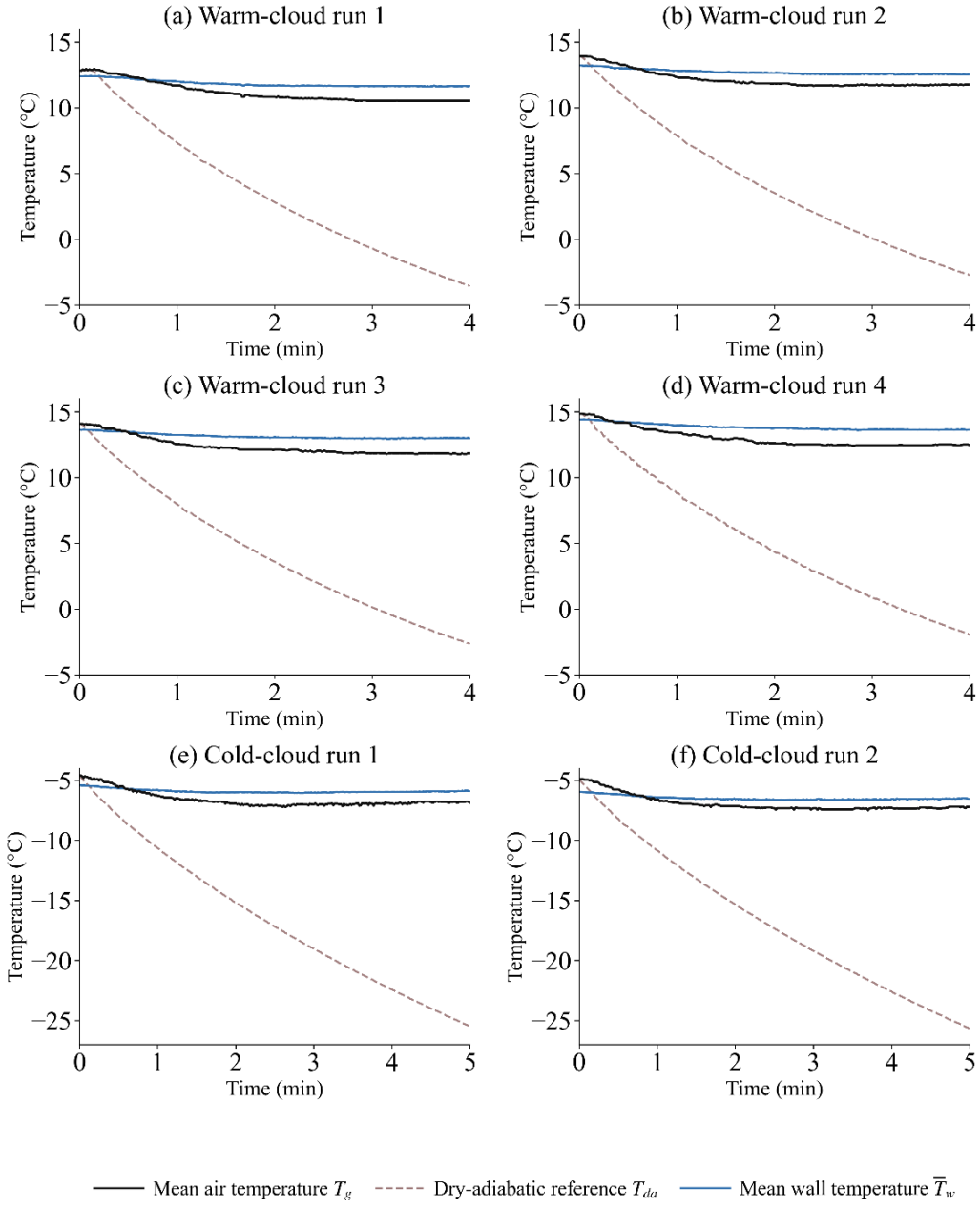

Major Comment 9

Aerosol measurements: size-range inconsistency, absent SMPS data, wet sizing, and in-cloud ambiguity (carried over from access review, point 5 - not addressed)

Response

We corrected the Bi-SMPS range, clarified the role of each particle instrument, and quantified their PSL sizing responses.

First, the previously inconsistent Bi-SMPS size range has been corrected. The Bi-SMPS used in this study is the Tsinghua University-developed bipolar scanning mobility particle sizer

described by Li et al. (2024). It uses naturally occurring positive and negative air ions for bipolar electrical-mobility sizing and consists of a differential mobility analyzer and a butanol-based condensation particle counter. Its nominal measurement range is 10–729 nm, which is now reported consistently in Table 2 and throughout the revised manuscript.

The revised manuscript also clearly distinguishes the roles of the particle instruments. The CUIT-Aerosol provided the aerosol number-concentration and size-distribution measurements shown in the warm- and cold-cloud experiments, whereas the FM-120 was used to characterize cloud-droplet size distributions. The Bi-SMPS and POPS were used for aerosol sizing characterization and intercomparison, including the PSL measurements presented in Fig. 2a. Accordingly, the aerosol time series in Figs. 7 and 8 are explicitly identified as CUIT-Aerosol measurements.

Second, the particle-sizing response is now quantified rather than assessed only from overlaid spectra. Duke PSL standards with nominal diameters of 200, 300, and 400 nm were measured using the Bi-SMPS, POPS, and CUIT-Aerosol. Supplement Table S1 reports the retrieved mean diameter, response width, and relative deviation from the nominal diameter for each instrument and PSL size. The instrument name has also been standardized throughout the manuscript as "CUIT-Aerosol."

Third, the sampling conditions have been clarified. Both the CUIT-Aerosol and Bi-SMPS were operated as external sampling instruments, with the sample stream passing through an inline drying tube before entering the corresponding sizing instrument. We nevertheless agree that optical measurements obtained under cloudy conditions should not automatically be interpreted as dry interstitial aerosol because hydrated particles and small activated droplets may not be unambiguously separated by optical sizing alone. The revised manuscript therefore no longer assigns the former in-cloud aerosol modes to specific dry-particle populations or uses them to infer seeding-related microphysical processes. Cloud-droplet characteristics are evaluated independently using the FM-120.

Finally, the FM-120 response was characterized using 5, 10, 15, and 30 μm PSL standards. Because PSL particles and water droplets have different optical properties, the retrieved values are reported as water-equivalent diameters and response widths within the manufacturer-defined Mie-based water-droplet sizing framework rather than as direct PSL sizing errors. No additional post-processing Mie correction was applied. The former CUIT-CDP calibration panels are no longer used to support the revised Results. The CUIT-Fog and CUIT-CIP measurements are not used to derive quantitative chamber-wide particle concentrations in the revised Results. The HCDS phase-classified time series is retained as supporting evidence discussed in Major Comment 5, but it is not used to derive a chamber-wide ice concentration or quantitative AgI glaciation efficiency.

The revised Fig. 2 and Supplement Tables S1 and S2 are reproduced below for clarity.

Revised Figure 2. Particle-sizing response characterization of the measurement instruments using PSL standards. (a) Response of Bi-SMPS, CUIT-Aerosol, and POPS to PSL particles with nominal diameters of 200, 300, and 400 nm. (b–e) FM-120 responses to PSL particles with nominal diameters of 5, 10, 15, and 30 μm.

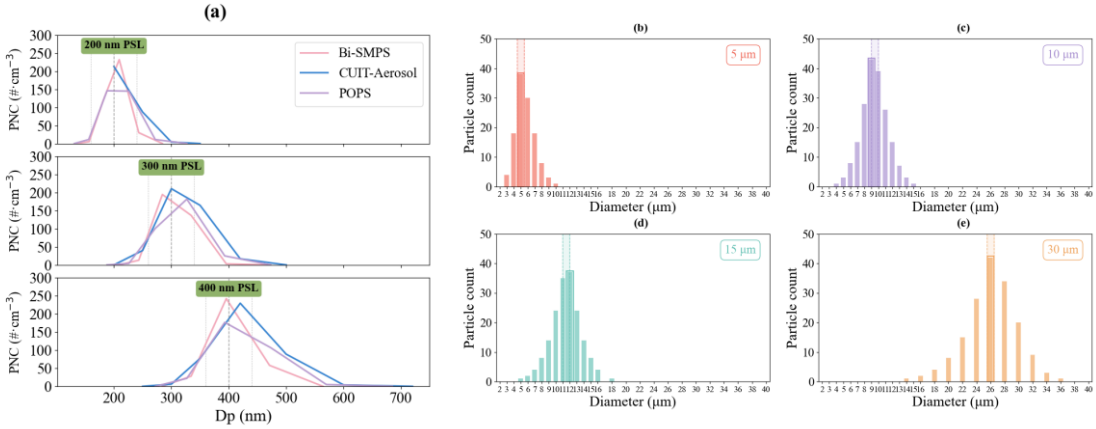

Supplement Table S1. Quantitative sizing-response characterization of the aerosol instruments using Duke PSL particle standards.

Nominal PSL diameter (nm)	Instrument	Retrieved mean diameter (nm)	Response width, σ (nm)	Relative deviation (%)
200	Bi-SMPS	202.52	18.11	+1.26
200	CUIT-Aerosol	215.63	24.55	+7.81
200	POPS	207.43	23.99	+3.72
300	Bi-SMPS	303.54	28.13	+1.18
300	CUIT-Aerosol	319.15	37.18	+6.38
300	POPS	313.19	35.61	+4.40
400	Bi-SMPS	403.75	35.45	+0.94
400	CUIT-Aerosol	424.26	53.35	+6.07
400	POPS	418.70	48.51	+4.68

Supplement Table S2. FM-120 sizing-response characterization using PSL standards.

Nominal PSL diameter (μm)	Total particle count	Retrieved mean water-equivalent diameter (μm)	Response width, σ (μm)
5	120	5.68	1.37
10	189	9.46	1.92
15	176	11.44	2.14
30	167	26.05	3.72

Major Comment 10

Background aerosol and chamber cleanliness (carried over from access review, point 6 - partially addressed, still insufficient)

Response

Chamber B was returned to near-ambient pressure after depressurization through a controllable bottom valve connected directly to the ambient environment. This refill pathway was not equipped with HEPA filtration, so the initial particle populations in the cloud-formation experiments were ambient-derived rather than composition-controlled clean-air backgrounds. The four warm-cloud experiments were conducted on 7 January 2026, and the two cold-cloud experiments on 2 August 2026. Their corresponding pre-depressurization aerosol number concentrations and size distributions are reported in Figs. 7 and 8.

Within each temperature-regime experiment set, the runs were conducted on the same day using the same ambient-air refill pathway and chamber-reconditioning procedure. However, no standardized clean-air flushing or post-cleaning aerosol baseline was established between runs. We therefore do not assume identical aerosol backgrounds within or between the two experiment sets, and no direct warm–cold aerosol-background comparison is made.

Particle wall-loss timescales, aerosol mixing time, chamber leak rate, and standardized post-cleaning background concentrations were not measured in these experiments and are not retrospectively corrected. Future chamber characterization will include dedicated wall-loss and mixing measurements, leak testing, and standardized post-cleaning background characterization before controlled aerosol experiments are interpreted quantitatively.

Major Comment 11

Sampling representativeness of the externally plumbed probes (new)

Response

We re-examined the particle-sampling configuration to clarify the spatial representativeness of the retained measurements. The lower section of chamber B was designed as the particle-observation region, where the in-situ FM-120 and HCDS measurements were performed. Such lower-section particle sampling is also used in other large cloud chambers; for example, cloud properties and several aerosol/cloud-particle instruments in the Manchester Ice Cloud Chamber are monitored or sampled in the bottom section (Connolly et al., 2012; Emersic et al., 2015). The measurements from chamber B are therefore used quantitatively to characterize the particle population sampled in the designated observation region. Because simultaneous particle measurements at multiple chamber heights were not available, however, we do not assume that a single observation level is identical to a strict chamber-volume-mean particle concentration.

The CUIT-Aerosol, which provides the aerosol number-concentration and size-distribution measurements retained in Figs. 7 and 8, was operated externally through a dedicated sampling line and inline dryer. It reports size-resolved aerosol measurements over 30 nominal diameter channels from 0.2 to 40 μm. The size-dependent aspiration and transmission efficiency of the complete chamber-to-instrument pathway was not independently characterized in these experiments. Accordingly, the CUIT-Aerosol data characterize the aerosol population delivered through the documented sampling pathway; possible size-dependent transport losses, particularly toward the larger particle channels, are not retrospectively corrected.

The CUIT-CDP, CUIT-Fog, and CUIT-CIP were also operated through external sampling pathways, whereas the FM-120 and HCDS were operated in situ within the designated lower observation region. The external-probe measurements are therefore interpreted with consideration of their sampling pathways and are not used to derive chamber-wide coarse-particle or ice-particle concentrations. The FM-120 and HCDS provide quantitative in-situ measurements within the designated observation region; however, in the absence of simultaneous multi-level particle measurements, these concentrations are not equated with strict chamber-volume-mean values. In particular, the HCDS phase-classified time series discussed in Major Comment 5 is not extrapolated to calculate a chamber-wide ice concentration or quantitative AgI glaciation efficiency.

Future chamber characterization will include dedicated aspiration/transmission tests for the external sampling pathways and simultaneous measurements at multiple chamber locations, where practicable, to quantify spatial representativeness before chamber-wide particle concentrations are reported.

Major Comment 12

The seeding materials themselves are unquantified (new)

Response

We have added the composition, introduced mass, hygroscopic response, and dry particle-size characteristics of the warm-cloud seeding material used in the original experiment.

The hygroscopic material was the optimized inorganic-salt formulation selected in the companion study by Jiang et al. Four candidate formulations were screened using static gravimetric moisture-uptake measurements, and the formulation used in the present chamber experiment, Formulation A, consisted of $CaCl_2$, NaCl, and $MgCl_2 \cdot 6H_2O$ at a mass ratio of 3:3:4. The actual mass of this material introduced in the original warm-cloud experiment was 10 g.

The hygroscopicity tests were conducted using a static gravimetric method under controlled conditions. At 25 °C and 100% RH, Formulation A showed the highest moisture uptake among the tested composite formulations, reaching approximately 310% under the reported test conditions (Fig. R12). This result provides a separate material-level characterization of the hygroscopic response of the formulation used in the chamber experiment.

The dry particle-size distribution of Formulation A was measured using a laser particle-size analyser. The reported volume-mean diameter was 54.238 μm (reported here as approximately 54.2 μm), with the main volume-frequency distribution concentrated around 50–60 μm (Fig. R13). These measurements characterize the dry material before introduction into the chamber.

The hygroscopicity and particle-size results reproduced in Figs. R12 and R13 are from the companion material-characterization study and refer to the same Formulation A used in the present warm-cloud experiment; they were not newly generated for this revision.

For the cold-cloud experiment, a commercially manufactured YF-4 aircraft flare produced by Shaanxi Zhongtian Rocket Technology Co., Ltd. was used. The reported 0.5 g refers to the actual mass of combustion material consumed during the experiment, rather than the mass of pure AgI. A batch-specific AgI mass fraction and the size/number distribution of the generated combustion aerosol were not available; therefore, the consumed material mass cannot be converted reliably into a net AgI mass or particle-number dose.

These additions provide quantitative material information for both seeding experiments while avoiding conversion of the nominal material dose into an unmeasured active-particle dose.

Figure R12. Time-dependent gravimetric moisture uptake of four composite formulations and reference salts at 25 °C and 100% RH. Formulation A ($CaCl_2$:NaCl:$MgCl_2 \cdot 6H_2O$ = 3:3:4) was the material used in the chamber experiment.

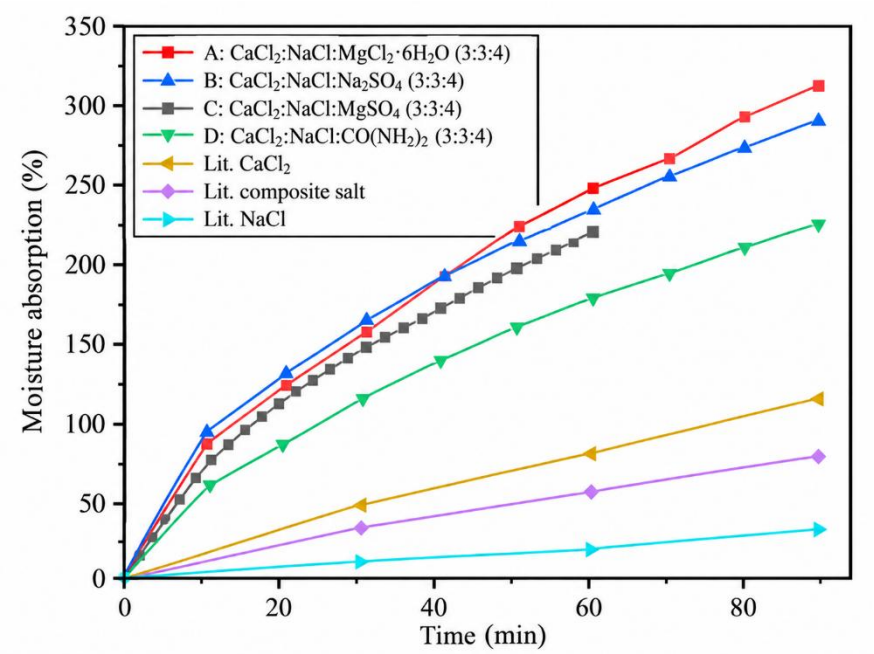

Figure R13. Dry volume-based particle-size distribution of Formulation A used in the chamber experiment.

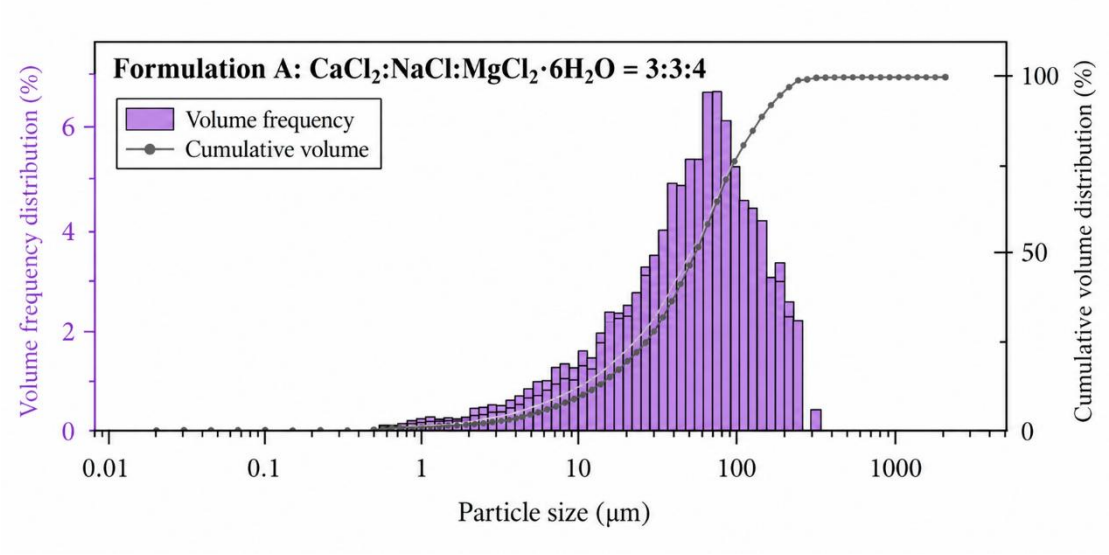

References

Anderson, J. C., Thomas, S., Prabhakaran, P., Shaw, R. A., and Cantrell, W.: Effects of the large-scale circulation on temperature and water vapor distributions in the Π Ch amber, Atmos. Meas. Tech., 14, 5473–5485, https://doi.org/10.5194/amt-14-5473-2021, 2 021.

Brunamonti, S., Saathoff, H., Hertzog, A., Diskin, G., Fujiwara, M., Rosenlof, K., Mö hler, O., Tuzson, B., Emmenegger, L., Amarouche, N., Durry, G., Frérot, F., Samake, J.-C., Cenac, C., Lopez, J., Monnier, P., and Ghysels, M.: The AquaVIT-4 intercompar

ison of atmospheric hygrometers, Atmos. Meas. Tech., 18, 5321–5348, https://doi.org/10.5194/amt-18-5321-2025, 2025.

Connolly, P. J., Emersic, C., and Field, P. R.: A laboratory investigation into the aggregation efficiency of small ice crystals, Atmos. Chem. Phys., 12, 2055–2076, https://doi.org/10.5194/acp-12-2055-2012, 2012.

DeMott, P. J.: Quantitative descriptions of ice formation mechanisms of silver iodide-type aerosols, Atmos. Res., 38, 63–99, https://doi.org/10.1016/0169-8095(94)00088-U, 1995.

Emersic, C., Connolly, P. J., Boult, S., Campana, M., and Li, Z.: Investigating the discrepancy between wet-suspension- and dry-dispersion-derived ice nucleation efficiency of mineral particles, Atmos. Chem. Phys., 15, 11311–11326, https://doi.org/10.5194/acp-15-11311-2015, 2015.

Gao, P., Wang, J., Zhao, C.-C., Tang, J.-B., Liu, J.-J., Yan, Q., and Hua, D.-X.: Simultaneous measurement of cloud microphysical parameters based on digital holographic interferometry, *Acta Phys. Sin.*, 70, 099201, https://doi.org/10.7498/aps.70.20201779, 2021 (in Chinese).

Gao, P., Wang, J., Tang, J., Gao, Y., Liu, J., Yan, Q., and Hua, D.: Investigation of cloud droplets velocity extraction based on depth expansion and self-fusion of reconstructed hologram, Opt. Express, 30, 18713–18729, https://doi.org/10.1364/OE.458947, 2022.

Jiang, Y., Xu, C., Ren, H., Wu, H., Su, Z., Deng, Y., Zhang, H., Luo, J., Li, Z., Li, Y., Guo, M., and Yang, C.: Laboratory and field studies on the fog-dissipation performance of a hygroscopic warm-cloud seeding agent, Journal of Arid Meteorology, accepted for publication, 2026 (in Chinese).

Li, Y., Wu, J., Wu, H., Liu, X., Zhou, Q., Lu, Y., Wu, Y., Liu, M., Ou, H., Mai, S., He, X., Song, H., Wang, H., Zeng, P., Wang, Y., Wang, D., Zhang, Q., Deng, J., Shi, J., Li, X., Zhao, J., Zhang, F., Huang, C., Zheng, M., Hao, J., and Jiang, J.: A bipolar SMPS network for measuring atmospheric aerosols using natural air ions, Atmos. Environ., 325, 120462, https://doi.org/10.1016/j.atmosenv.2024.120462, 2024.

Moteki, N. and Kondo, Y.: A new theoretical method for calculating temperature and water vapor saturation ratio in an expansion cloud chamber, J. Geophys. Res.-Atmos., 118, 6633–6642, https://doi.org/10.1002/jgrd.50517, 2013.

Yang, C. Y., Wang, J., Zhang, C., Zhou, H., Yang, J. S., Yue, Z. G., Liang, G., Liu, J. J., and Hua, D. X.: Observation method of microphysical parameters of ice crystals

in cloud based on digital holography, *Acta Optica Sin.*, 44, 0601017, https://doi.org/10.3788/AOS231067, 2024 (in Chinese).

Minor Comment 1

Sect. 2.2 / Fig. 3b: nearly every number in the text is contradicted by the figure. The text gives 102 min at 0 °C + 110 min (0 → −10 °C) + 4 min hold at −10 °C + a 189-min descent to −20 °C + 30 min at −20 °C, but the figure ends at approximately 200 min. Please re-derive this entire paragraph from the experimental record and restate the plateau-stability claims accordingly.

Response

We thank the Reviewer for identifying the inconsistencies between the previous description of the temperature-gradient experiment and Fig. 3b. We re-examined the temperature record and have completely revised the corresponding description so that the reported timing and temperature evolution are consistent with the experimental data shown in Fig. 3b.

In the revised manuscript, the previous descriptions of a 110 min transition from 0 to −10 °C, a 4 min hold at −10 °C, a 189 min descent to −20 °C, and a 30 min hold at −20 °C have been removed. The revised text now states that the 210 min record shows chamber B initially maintained near 0–2 °C for approximately 105 min, followed by rapid cooling to approximately −10 °C within several minutes, a quasi-stable period near −10 to −11 °C for about 30 min, and subsequent cooling toward approximately −20 °C near the end of the record.

We have also revised the description of vertical temperature uniformity. Rather than assigning a single restrictive inter-level temperature-difference threshold to the entire experiment, the revised manuscript now states that the upper-, middle-, and lower-level temperature records exhibited broadly consistent temporal evolution, with relatively small inter-level differences during quasi-stable stages and larger differences occurring mainly during rapid cooling transitions. This revised description is consistent with the temporal behaviour shown in Fig. 3b.

Changes in manuscript

Section 2.2, Fig. 3b: The temperature-gradient-test description has been re-derived and rewritten to match the experimental record. The previous inconsistent stage durations and overly restrictive thermal-uniformity statement have been removed.

Minor Comment 2

Thermal-uniformity statements need tightening: L190-191 claims vertical differences < 0.3 degC, L192 claims < 1 degC; state clearly which applies under which conditions, and translate the +/-0.5-1 degC spread into the corresponding equilibrium-RH inhomogeneity (~+/-3-7 % near saturation), which is directly relevant to Major comments 3 and 7.

Response

We thank the Reviewer for identifying this ambiguity. The previous statements mixed two different operating conditions. In the revised manuscript, the former <0.3 °C statement has been

removed. During the quasi-steady temperature-stability test shown in Fig. 4, the temperature difference between adjacent air-temperature levels remained within approximately 1 °C. During active cloud-forming depressurization, larger vertical temperature differences developed: the mean inter-level temperature ranges were 0.87–1.01 °C for the four warm-cloud runs and 1.15–1.27 °C for the two cold-cloud runs.

We also agree that this thermal inhomogeneity is directly relevant to the interpretation of humidity near saturation. At approximately fixed water-vapour pressure, the local equilibrium RH varies inversely with saturation vapour pressure. Near 0 to −10 °C, a local temperature deviation of approximately ±0.5–1 °C corresponds to roughly ∓3–7 percentage points in RH near saturation, with warmer regions having lower RH and colder regions higher RH. Thus, a single-point RH measurement should not be interpreted as an exact chamber-volume-mean humidity state during cloud formation. We have clarified this limitation in the revised manuscript and in our responses to Major Comments 3 and 7.

Minor Comment 3

Chamber A / differential-pressure mode is described at length (Sect. 2.1, Table 1, Fig. 1) but never demonstrated. State explicitly that the dual-vessel mode is untested and defer performance claims for it.

Response

We agree that the previous manuscript did not clearly distinguish between the designed capability of the dual-vessel system and the operating configuration actually evaluated in this study.

All performance tests and cloud-formation experiments reported in the revised manuscript were conducted exclusively in chamber B, with the interconnecting valves between chambers A and B kept closed. The coupled differential-pressure mode between the two chambers is a designed capability of the facility, but it was not experimentally evaluated in the present study.

Chamber A and the differential-pressure configuration are therefore retained in Fig. 1 and Table 1 only as part of the facility design description, and no performance claim is made for coupled dual-vessel operation.

Changes in manuscript

Section 2.1 now explicitly states that all reported experiments were conducted in chamber B with the interconnecting valves closed and that coupled differential-pressure operation between chambers A and B was not evaluated in this study.

Minor Comment 4

L285 “Larger droplets then formed through collision-coalescence and condensational growth”:

collision-coalescence is negligible for a quiescent 3–10 μm population on ~5 min timescales; remove or substantiate.

Response

We agree that the collision–coalescence interpretation was not sufficiently supported by the measurements or the experimental timescale.

This mechanistic interpretation has therefore been removed from the revised manuscript. The revised Results now report only the directly observed droplet-size characteristics measured by the FM-120, without attributing the observed size evolution to collision–coalescence or to any other specific growth mechanism. For the four warm-cloud experiments, the dominant droplet populations are described as being concentrated mainly within the 3–10 μm size range, with the highest channel-resolved concentrations generally occurring near 5 μm.

This revision limits the interpretation to what is directly supported by the measurements and avoids assigning an unsupported microphysical mechanism to the observed droplet-size distributions.

Changes in manuscript

Section 3.1: The previous statement attributing larger-droplet formation to collision–coalescence and condensational growth has been removed. The revised text now describes only the measured droplet-size distributions and does not assign a specific growth mechanism.

Minor Comment 5

Figs. 7/9 (a–d): define the plotted quantity (per-bin concentration vs$dN/d\log D_p$), the bin widths, and the instrument used for the droplet panels.

Response

We have clarified both the measurement instrument and the plotted quantity in the revised figures. The aerosol panels are based on CUIT-Aerosol measurements, whereas the droplet panels are based on FM-120 measurements.

For the CUIT-Aerosol, the colour scale represents the instrument-reported number concentration in each predefined size channel (cm^{-3}). For the FM-120, the raw export provides the total number concentration together with particle counts in 30 predefined size channels. The per-channel droplet number concentration was therefore calculated for each record as

$$N_i = N_{\mathrm{tot}} \frac{C_i}{\sum_j C_j},$$

where $N_{\mathrm{tot}}$is the FM-120 total number concentration and C_i is the particle count in channel

i. The colour scale in the droplet panels therefore represents per-channel number concentration (cm^{-3}), rather than raw particle counts.

The available instrument files provide nominal channel diameters but not independently verified lower and upper channel boundaries. We therefore use nominal channel diameter as the size coordinate and do not report unverified bin widths. Accordingly, the plotted quantities are per-channel number concentrations and are not normalized by channel width or presented as $dN/d\log D_p$.

Minor Comment 6

The cold and warm backgrounds differ by a factor of ~5; a sentence comparing the two ambient situations (and their dates) is needed for the paired-design logic to be assessable.

Response

We appreciate the Reviewer's comment. In the revised manuscript, the former paired background–seeded design and the associated seeding-effect comparison have been removed. The warm-cloud and cold-cloud experiments are now presented as separate chamber-operation demonstrations rather than as directly paired aerosol-background cases.

We have clarified that the initial particle populations in these experiments were derived from ambient air and were not composition controlled. The four warm-cloud experiments were conducted on 7 January 2026, whereas the two cold-cloud experiments were conducted on 2 August 2026. Because these two experiment sets were performed on different dates under different ambient atmospheric conditions, their aerosol backgrounds are not expected to be directly comparable.

We have therefore added a sentence clarifying that the warm- and cold-cloud aerosol backgrounds may differ substantially in concentration and size distribution and that no direct cross-regime aerosol-background comparison is made in the revised manuscript.

Changes in manuscript

Section 2.2: The manuscript now states that the warm- and cold-cloud experiments were conducted on different dates using ambient-derived aerosol backgrounds and clarifies that these backgrounds are not used for direct comparison between the two temperature regimes.

Minor Comment 7

Fig. 5: annotate the shaded bands; y-axis "Humidity (%)" → "Relative humidity (%)"; the caption lacks a final period. The abstract's "nearly the full 0 to 100 % range" should be reconciled with the demonstrated 10.3–98.4 %.

Response

We appreciate the Reviewer's careful comments on Fig. 5 and the corresponding description of the humidity-control performance.

In the revised figure, the shaded intervals are now explicitly labelled as the pressurization and depressurization stages, and the right-hand y-axis has been changed from "Humidity (%)" to "Relative humidity (%)". The figure caption has also been corrected and now ends with a final period.

We have additionally removed the previous statement in the Abstract that described the demonstrated humidity-control range as "nearly the full 0 to 100 % range". The revised manuscript now reports only the experimentally demonstrated values. Specifically, the relative humidity decreased from approximately 98.4 % to 10.3 % during the drying test and subsequently increased to approximately 96.8 % during re-humidification.

Changes in manuscript

Figure 5 and Abstract: The shaded operating stages in Fig. 5 are now labelled, the humidity axis is given as "Relative humidity (%)", and the caption punctuation has been corrected. The previous "nearly the full 0 to 100 % range" statement has been removed from the Abstract, and only the demonstrated RH range is reported in the revised manuscript.

Minor Comment 8

Data availability: the Mendeley record should be verified to contain the raw data behind Figs. 2–9, including the raw holograms and the processing/reconstruction code; at present the paper's key claims cannot be independently re-derived.

Response

We have reviewed and reorganized the Mendeley Data repository so that it corresponds directly to the revised manuscript. The repository contains the experimental datasets underlying the figures and quantitative analyses retained in the revised paper, including the data supporting Figs. 2–9 and the corresponding supplementary sizing-response analyses. The dataset is publicly available at https://doi.org/10.17632/6zszgtcdd4.2 (Luo, 2026).

The revised manuscript no longer includes the original seeding-effect comparisons, quantitative supersaturation analysis, or hologram-based AgI glaciation analysis as principal results. The public data package has therefore been organized around the datasets required to reproduce the analyses and figures that remain in the revised manuscript.

The complete acquisition-level raw hologram archive from the original AgI demonstration was not retained in the working dataset and therefore cannot be provided retrospectively. The HCDS data available from that experiment consist of the retained processed 1 s outputs described in our response to Major Comment 5. The hologram reconstruction and phase-classification

processing was performed using the established instrument-specific analysis software developed at Xi'an University of Technology and described by Yang et al. (2024). The underlying software source code is not part of the retained dataset for the present study and is therefore not included in the repository.

Importantly, no quantitative conclusion in the revised manuscript depends on the superseded AgI hologram analysis. The revised Data availability statement therefore refers to the public dataset supporting the figures and quantitative analyses retained in the final manuscript:

"The dataset is publicly available at https://doi.org/10.17632/6zszgtcdd4.2 (Luo, 2026)."

Technical Correction 1

Title: remove "Quantitative" (see Major comment 1).

Response:
Thank you for this suggestion. "Quantitative" has been removed from the title, which has been revised to **"Design and Characterization of a Cloud Chamber for Warm- and Cold-Cloud Microphysical Studies."**

Technical Correction 2

Sect. 2.1 (L92-108): words are broken across lines without hyphens ("chambe r B", "optic al windows", "differentia l-pressure", "mechanica l vacuum pump", "botto m valve") - please fix the typesetting throughout.

Response:
Thank you for pointing this out. The unintended word breaks in Sect. 2.1 and similar typesetting errors throughout the manuscript have been corrected.

Technical Correction 3

Terminology: "catalyst/catalytic/flame-based catalysts" persists throughout (L106-107, Fig. 1a labels, L252-266, L363, L371) despite the access-review correction; the accepted terminology is "seeding material/agent". The section titles were fixed; the body text was not.

Response:
Thank you for this correction. The terminology has been revised throughout the manuscript, and the previous expressions "catalyst", "catalytic", and related terms have been replaced with "seeding material" or "seeding agent", where applicable.

Technical Correction 4

L273-274: a figure caption has been pasted into the running text ("Fig. 6 Sequential images of warm-cloud formation ... after cloud formation."), producing a broken sentence; the actual Fig. 6 caption still lacks the (a)-(c) panel descriptions.

Response:

Thank you for pointing this out. The misplaced Fig. 6 caption has been removed from the running text, and the revised caption now clearly identifies panels (a)–(c) and their corresponding times relative to the onset of depressurization.

Technical Correction 5

Fig. 2: legend "PSD" vs caption "CUIT-Aerosol" (unify); double space in "(b-e) Calibration"; state the calibration particle material (see Major comment 9).

Response:

The Fig. 2 legend has been standardized to “CUIT-Aerosol,” the spacing in “(b–e) Calibration” has been corrected, and the calibration material is identified as Duke polystyrene latex (PSL) particle standards in both the figure and caption.

Technical Correction 6

Table 2: "Manufacture" -> "Manufacturer" (and the column mostly lists instrument acronyms, not manufacturers - the CUIT instruments should name the developing laboratory); "0-60 mmol" -> presumably mmol/mol (and give the CO2 range or drop the CO2 mention); the HCDS sample volume is missing; velocity vs flow-rate units (see Major comment 11); "-60-160 degC" formatting.

Response:

Table 2 has been revised to replace “Manufacture” with “Manufacturer,” identify the manufacturers/developing institutions of the CUIT instruments, correct the concentration and velocity/flow units, add the 5 cm^3 HCDS observation volume, and standardize the formatting of the measurement ranges. The former CO_2 entry has also been removed because it is not used in the present analysis.

Technical Correction 7

Fig. 4 caption: "Figure 4," -> "Figure 4."; the caption ("Wall Temperature stability") mislabels panel (a), which shows air temperature; capitalization.

Response:

Thank you for pointing this out. The Fig. 4 caption has been corrected to distinguish the air-temperature stability test in panel (a) from the wall-temperature stability test in panel (b), and the caption formatting has been revised accordingly.

Technical Correction 8

Fig. 8: define the reference time of "after 1 min" in the caption; move the solid/dashed in-image circle legend into the caption; state the hologram frame dimensions, pixel resolution, and depth

of field.

Response:

Thank you for this comment. The former HCDS-based Fig. 8 and the associated particle-phase interpretation have been removed from the revised manuscript. The revised Fig. 8 now presents the two repeated cold-cloud formation experiments; therefore, the former requests concerning hologram timing, circle annotations, frame dimensions, and depth of field are no longer applicable to the revised figure.

Technical Correction 9

Overprecise single-run averages (117.44 / 72.60 hPa/min; 26.84 / 27.72; 32.63 / 32.91; 1357 / 478): round to a defensible precision and define the averaging windows (the P(t) curves are visibly nonlinear).

Response:

Thank you for this comment. The former 1357/478 cm^{-3} values have been corrected through the raw-data re-analysis described in Major Comment 4, where the exact averaging intervals are now provided. These former single-pair values remain excluded from the revised manuscript as evidence of a seeding effect. Other retained numerical values have been rounded to a precision appropriate to the measurements.

Technical Correction 10

L320 "at 16:41": replace with time relative to expansion onset (see Major comment 6).

Response:

Thank you for this correction. The former AgI experiment and its absolute-time injection description have been removed from the revised manuscript; therefore, the statement “at 16:41” is no longer present.

Technical Correction 11

L360-361: "temperature, humidity, pressure, and water vapour" - humidity and water vapour are redundant here.

Response:

Thank you for pointing this out. The redundant wording referring separately to both “humidity” and “water vapour” has been removed in the revised manuscript.

Technical Correction 12

References: Schnitzhofer et al. is cited as 2013 in the text (L59) and dated 2013 in the list, but the DOI (amt-7-2159-2014) is from 2014; fix both. Khain et al. (2024) is given an SSRN preprint DOI for a J. Weather Modif. article; verify the final metadata. Data availability:

"(Luo,2025)" is missing a space.

Response:

Thank you for these corrections. The Schnitzhofer et al. citation has been corrected to 2014, the reference list has been rechecked and updated, and the Data availability citation has been revised to the current dataset record, Luo (2026). The SSRN preprint DOI previously attached to Khain et al. has been removed and the reference has been replaced with the final Journal of Weather Modification article metadata.

Technical Correction 13

Acronyms AIDA, CLOUD, MRI, K-CPEC are undefined at first use (L53-63).

Response:

Thank you for this comment. The relevant acronyms are now defined at first use, including Aerosol Interaction and Dynamics in the Atmosphere (AIDA), Cosmics Leaving OUtdoor Droplets (CLOUD), and Korea Cloud Physics Experimental Chamber (K-CPEC). MRI is no longer used as an undefined acronym in the running text.

Technical Correction 14

L92-93: the stated chamber-B dimensions (1.8 m diameter x 3.6 m height cylinder) give ~9.16 m^3, outside the stated 9.0 +/- 1 %; presumably head geometry - please clarify.

Response:

Thank you for pointing out this apparent inconsistency. The vessel has an overall internal height of 3.6 m, including an approximately 2.8 m straight cylindrical section and the upper and lower ellipsoidal heads. The 9.0 m^3 value is the manufacturer-specified nominal internal volume.

Technical Correction 15

Financial support: missing spaces ("Project(2025ZYD0179),the", "Administration(CMA ...").

Response:

Thank you for pointing this out. The spacing and formatting errors in the Financial support section have been corrected.

Technical Correction 16

Redundancy: the "initialized from the same ambient aerosol source" statement appears three times nearly verbatim (L244-249, L267-269, L316-318); condense.

Response:

Thank you for this comment. The repeated statements concerning the ambient-derived aerosol background have been condensed. The revised Methods now provides the main description of the ambient-air refill and background conditions, while the Results retain only brief information

needed to identify the initial aerosol background for each experiment set.